R. WŁODARCZYK*, A. DUDEK**, Z. NITKIEWICZ**

CORROSION ANALYSIS OF SINTERED MATERIAL USED FOR LOW-TEMPERATURE FUEL CELL PLATES

ANALIZA KOROZYJNA MATERIAŁÓW SPIEKANYCH PRZEZNACZONYCH DO NISKOTEMPERATUROWYCH OGNIW PALIWOWYCH

A significant part of proton exchange membrane fuel cells (PEMFC) stack is the bipolar plates (BPs), which account for about 80% of total weight and 45% of stack cost. They are designed to accomplish many functions, e.g. they distribute reactants uniformly over the active areas, remove heat from active areas, carry current from cell to cell and prevent leakage of reactants and coolant. Furthermore, the plates must be of inexpensive, lightweight materials and must be easily manufactured.

Materials designed for interconnectors must, among other things, be characterized by resistance to corrosion in the environment with pH= 2-3. This study presents opportunities of use of sintered stainless steel for this part of fuel cells. Resistance to corrosion of sintered materials was compared to properties of material (with the same ferritic phase composition) manufactured in conventional way (plastic forming), i.e. X20Cr13 stainless steel.

Keywords: fuel cell, bipolar plates, sintering steel, corrosion

Ważnym elementem budowy ogniw paliwowych z membraną jonowymienną są okładki/interkonektory. Okładki ogniw paliwowych stanowią około 80% masy całkowitej oraz 45% ceny ogniwa. Okładki do ogniw paliwowych muszą być zaprojektowane tak, aby spełniały wiele funkcji, takich jak jednorodna dystrybucja reagentów w obszarach aktywnych, przewodzenie prądu pomiędzy ogniwami i zabezpieczenie przed wyciekiem reagentów i medium chłodzącego. Poza tym okładki muszą być wykonane z tanich, łatwych w produkcji materiałów o małej masie.

Materiały przeznaczone na interkonektory muszą między innymi charakteryzować się odpornością na korozję w środowiskach o pH= 2-3. W pracy przedstawiono możliwości zastosowania spiekanej stali nierdzewnej na ten element ogniwa paliwowego. Odporność na korozję materiału spiekanego porównano z własnościami materiału (posiadającego jednakową strukturę fazową, tj. ferrytyczną) wytwarzanego w sposób tradycyjny (tj. po obróbce plastycznej) – stali nierdzewnej X20Cr13.

1. Introduction

The concept of conventional fuel cell is show in Fig. 1. A fuel cell consists of two electrodes sandwiched between a membrane/electrolyte [1-5]. Most often, hydrogen is used as the fuel in fuel cells. The hydrogen reacts with oxygen from the air in such a way that a voltage is generated between the two electrodes [6]. The reactions occur in a chemical medium referred to as electrolyte (ion conducting membrane) in the presence of catalysts.

Hydrogen fuel is fed to the anode of the fuel cell. Oxygen (or air) enters the fuel cell through the cathode. The hydrogen atom splits into a proton and an electron at the anode due to the presence of catalysts (see Fig. 1). These protons and electrons return to the cathode through the electrolyte and the outer path (external load), respectively. The electrons create a separate current in the outer path, which can be utilized before the electrons return to the cathode. These electrons are united with the protons and oxygen to form a molecule of water (waste of fuel cell emissions).

The overall reaction of the fuel cell is:

fuel + oxidant → oxidation products + work + heat rejected.

* CZESTOCHOWA UNIVERSITY OF TECHNOLOGY, DEPARTMENT OF ENERGY ENGINEERING, 42-200 CZĘSTOCHOWA, 19 ARMII KRAJOWEJ STR., POLAND

** CZESTOCHOWA UNIVERSITY OF TECHNOLOGY, INSTITUTE OF MATERIALS ENGINEERING, 42-200 CZĘSTOCHOWA, 19 ARMII KRAJOWEJ STR., POLAND
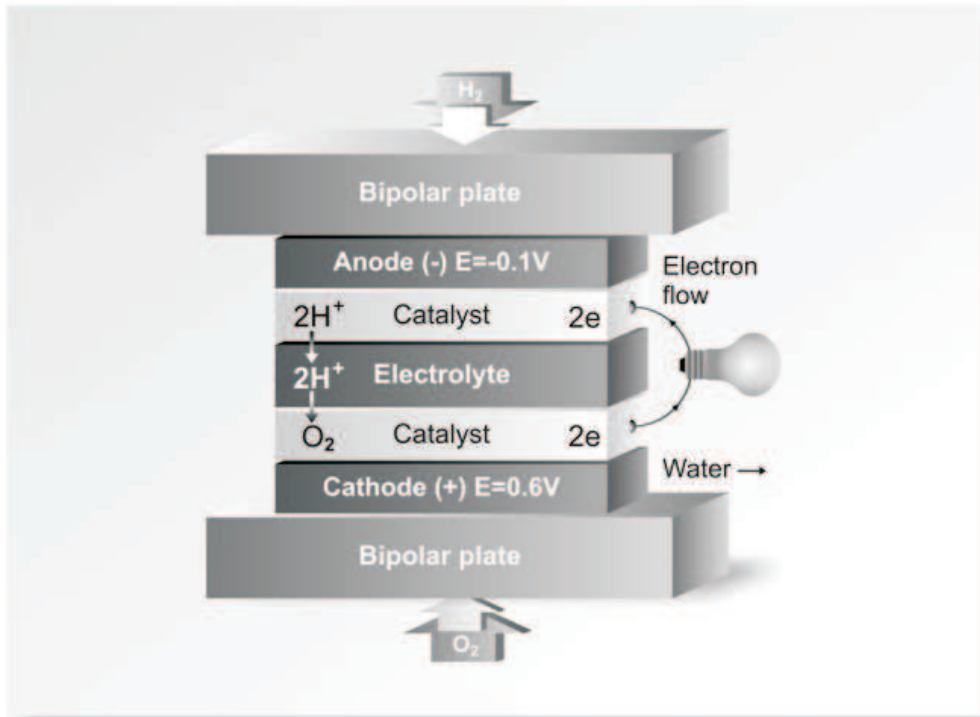
Fig. 1. Concept of fuel cell system

PEM fuel cell (Fig. 1) essentially consist of an anode backing, electrode assembly (MEA) and cathode backing sandwiched between two BPs. The BPs have the following functions to perform:

– to distribute the fuel and oxidant within the cell,
– to facilitate water management within the cell,
– to separate individual cells in the stack,
– to carry current away from the cell,
– to facilitate heat management.

Hence, the materials that BPs are made of would have different physical and chemical properties related to each function [7-10]. Important physical and chemical properties of BP materials are:

– coefficient of thermal expansion,
– density,
– hydrophobicity,
– electrical and thermal conductivity,
– H_2 permeability,
– corrosion resistance.

Mehta and Cooper [9] have suggested precisely the criteria of properties. As mentioned before, materials for BPs are expected to show improved resistance to corrosion. BPs are exposed to an operating environment with the a pH of 2-3 at the temperatures of around 80°C. The dissolved metal ions may lead to poisoning of PEM membrane and hence lowering of ionic conductivity. Moreover, a corrosion layer on the surface of a BP increase the electrical resistance and decreases the output of the cell. In the light of these issues, two types of metallic plates have been studied, steel produced using conventional methods and sintered steel. Properties of 434LHC sintered steel were compared to X20Cr13 steel, which also has ferritic structure. X20Cr13 steel is widely used for parts e.g. in energy equipment.

Experimental Part

Percentage composition of the investigated materials is presented in Table 1. The 434LHC powder was compacted with the load 765 MPa and sintered at the temperature of 1250°C for 30 minutes in ammonia medium.

TABLE 1

Chemical composition of the materials

Materials	C [%]	Mo [%]	Ni [%]	Cr [%]	Si [%]	Mn [%]	Fe [%]
X20Cr13 steel	0.2	–	–	12.6	0.3	0.3	balance
434 LHC sinter	0.015	0.98	–	16.2	0.8	0.1	balance

In order to assess the impact of the technology of material preparation (conventional preparation method with heat processing or sintering), polarization curves were registered in the following solutions: 0.1 mol dm^{-3} H$_2$SO$_4$, 0.5 mol dm^{-3} H$_2$SO$_4$ 0.5 mol dm^{-3} Na$_2$SO$_4$ (pH=4) and 0.5 mol dm^{-3} Na$_2$SO$_4$+ 0.5 mol dm^{-3} NaCl (pH=4), scan rate of 1 mV s^{-1}. On the basis of polarization curves, the parameters which define corrosion resistance of the material were determined, i.e. corrosion potential E_{corr}, corrosion current density i_{corr}. The most representative polarization curves were used for analysis of corrosion resistance. Electrochemical measurements were carried out in three-electrode arrangement by means of CHI660 (CH Instruments USA) measurement unit. Reference electrode was formed by saturated calomel electrode (SCE) while auxiliary electrode was platinum wire. The sample was then placed just above the tip of the luggin capillary (approximately 2–3 mm). All chemicals were reagent grade and were used as received without further purification. Distilled and subsequently deionized water was used to prepare test solutions. Scanning electron microscopy (SEM) images were obtained using JOEL Model JSM-5400.

2. Test results and discussion

Microstructural tests

On the basis of the morphological analysis of 434LHC powder, it was found that average grain size was ca. 50 μm while the powder density was assessed to be ca. 2.6 g/cm^3. 434LHC powder microstructure and 434LHC sinter microstructure is presented in Fig. 2.

Fig. 2. Morphology of 434LHC powder, magnification 200x (A), Microstructure of 434LHC sinter, magnification 200x (B)

TABLE 2

Properties of the powder and obtained sintered steel

Powder Grade	Density [g cm^{-3}]	Powder Density [g cm^{-3}]	Grain Size [μm]
X20Cr13 steel	7.86	–	–
434 LHC sinter	6.60	2.87	∼ 50

In the case of steel powder (Fig. 2A), geometric parameters were determined, i.e. perimeter and roundness. The results are presented in the form of histograms in Fig. 3. The powders with dendritic shape are characterized by increased degree of surface development (average 1.97) whereas mean value of the perimeter amounts to 342 μm.
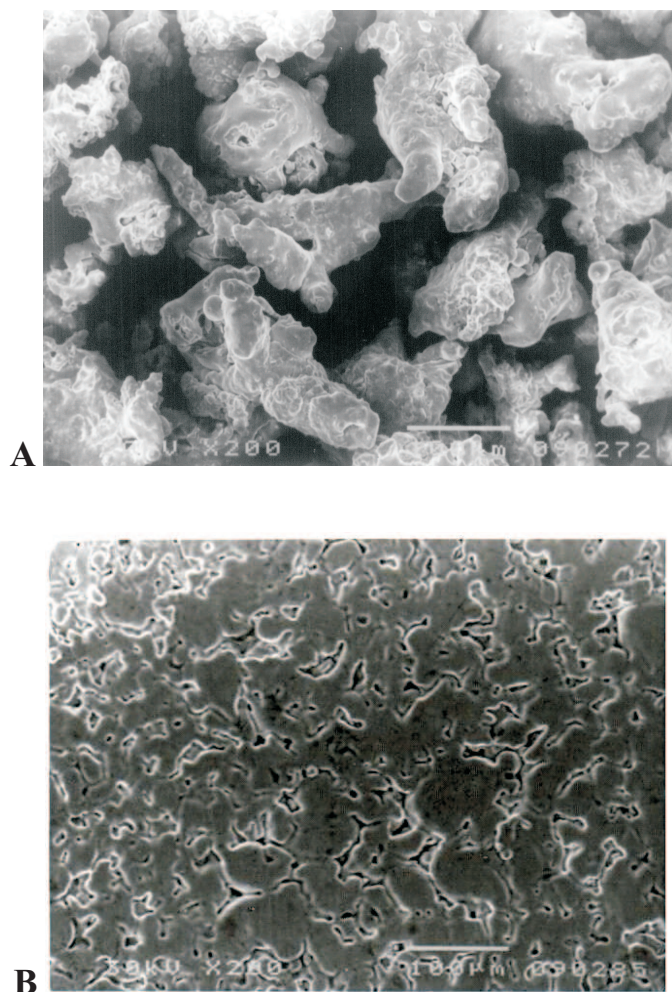
On the basis of microstructural tests carried out for stainless steel after sintering (Fig. 2B), porosity of the investigated sinter was evaluated to be at the level of 11%. The analysis also concerned pore surface revealed in the sintered steel and the observed roundness. As results from the histogram presented in Fig. 4A, ca. 75% of pores are within the range of 50 μm^2 to 100μm^2 (including 50% of pores with surface area of ca. 50 μm^2). As results from the distribution presented in Fig. 4B, pores are typically of irregular shape (roundness up to 2 for 80% of the population) but more complex-shaped pores also exist, which proves higher values of roundness (up to 11).
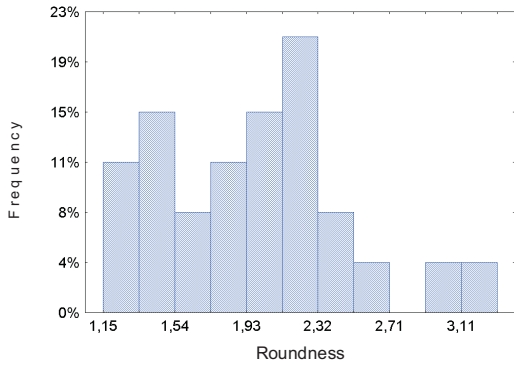
R shape factor was calculated as:

$$R = \frac{L^2}{2\pi A} \qquad (1)$$

where L – particle perimeter, A – particle surface area. The shape factor determines development of the surface of a particle (for the particle with round cross-section, R=1).
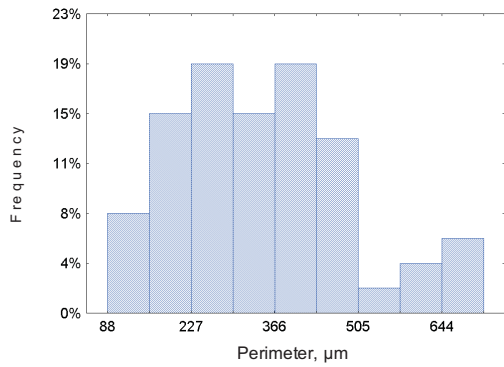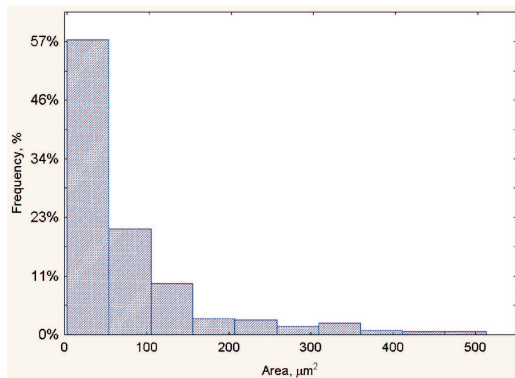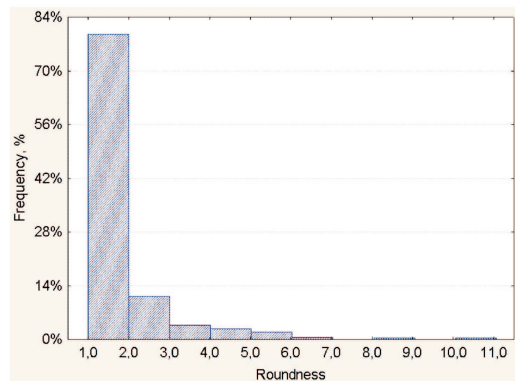
A

B

Fig. 3. Histogram of perimeter in 434LHC powder particles (A); Histogram of roundness shape factor in 434LHC powder particles (B)


A

B

Fig. 4. Distribution of surface area for cross-sections of pores (A), distribution of roundness in the sintered material (434LHC steel) (B)

3. Corrosion resistance tests

In order for corrosion resistance properties in X20Cr13 steel to be compared with 434LHC sintered material, potentiokinetic curves were registered in sulphate solutions with concentration of 0.1 mol dm^{-3} H_2SO_4 (Fig. 5A) in 0.5 mol dm^{-3} solution of H_2SO_4 (Fig. 5B). As observed on the basis of potentiokinetic curves, steel materials (X20Cr13 and 434LHC) show similar values of corrosion potentials, i.e. -0.52V vs. SCE in 0.1 mol dm^{-3} H_2SO_4 and -0.51V vs. SCE in 0.5 mol dm^{-3} H_2SO_4. Differences in potentiokinetic curves were observed within cathode range. In the case of steel produced using conventional methods, values of current densities within the investigated range are higher and, in 0.5 mol dm^{-3} solution of H_2SO_4 amount to 45.4 ma cm^{-2} for X20Cr13 steel and 9.22 mA cm^{-2} for 434LHC sinter.
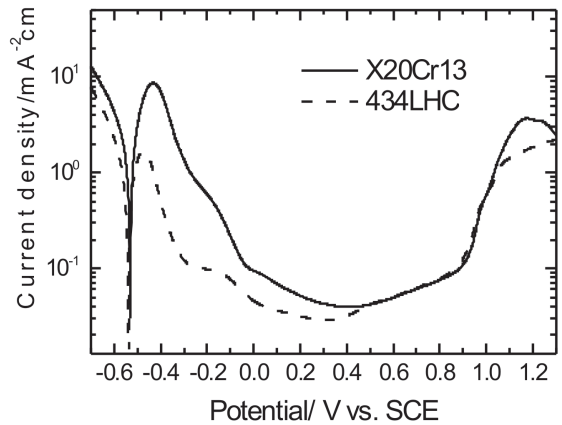
A
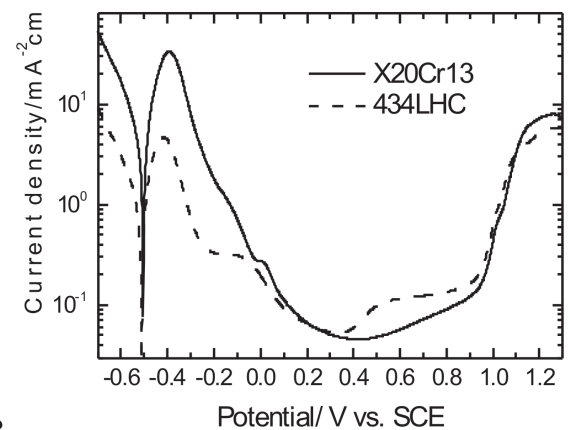
B

Fig. 5. Anodic polarization curves for sintered stainless steel obtained in 0.1 mol dm^{-3} H_2SO_4 (A), 0.5 mol dm^{-3} H_2SO_4 (B), scan rate 1 mV s^{-1}

Type of steel affected the value of current density corresponding to the potential in the initial point of pas-

sivation. The values of current densities in both solutions of 0.1 mol dm^{-3} H$_2$SO$_4$, and 0.5 mol dm^{-3} H$_2$SO$_4$, are nearly eight-time lower for sintered steel as compared to X20Cr13. After exceeding of the value of potential in the initial point of passivation, anode current densities are lower in sintered steel. The investigated materials are subject to passivation in sulphate solutions, whereas passive layer breakthrough potential is similar for both materials and amounts to ca. 0.9V vs. SCE, (both in 0.1 mol dm^{-3} H$_2$SO$_4$, as well as in 0.5 mol dm^{-3} H$_2$SO$_4$).

A

B
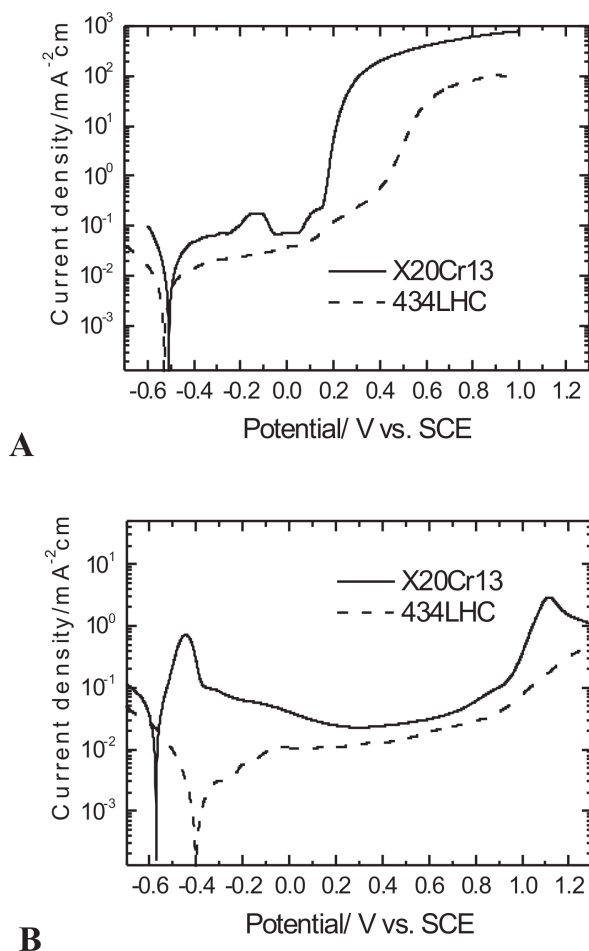
Fig. 6. Anodic polarization curves for sintered stainless steel obtained in 0.5 mol dm^{-3} Na$_2$SO$_4$ (A), 0.5 mol dm^{-3} Na$_2$SO$_4$ + 0.5 mol dm^{-3} NaCl (B), scan rate 1 mV s^{-1}

Polarization curves registered in 0.5 mol dm^{-3} Na$_2$SO$_4$ are presented in Fig. 6A. X20Cr13 steel with ferritic structure and 434LHC sinter, also with the structure of ferrite, show similar corrosion potential in the investigated solution equal to E_{corr}= -0.5V vs. SCE. The values of current densities in the cathode and anode ranges are lower for the sinter and, after exceeding of potential of 0.4V vs. SCE (in 434LHC sinter) and 0.2V vs. SCE (in X20Cr13 steel), current density rises rapidly for both materials.

In order to assess the impact of the method of material preparation (sintering, conventional steel manufacturing) on pitting corrosion in steels, potentiokinetic curves were registered in 0.5 mol dm^{-3} Na$_2$SO$_4$ + 0.5 mol dm^{-3} NaCl (Fig. 6B). Potentiokinetic curves clearly prove that the steel manufactured by means of powder metallurgy shows higher resistance to aggressive chloride ions. Corrosion potential for the material amounts to -0.41V vs. SCE and is by 0.18V higher than corrosion potential registered for X20Cr13 steel. Values of currents are lower than for sintered steel within the measurement range (-0.6V to 1.2V vs. SCE).

As results from the data presented in Table 3, stainless steel manufactured by means of powder metallurgy (compaction, sintering) shows improved corrosion-resistance properties in the investigated environment as compared to stainless steel manufactured conventionally with comparable ferritic structure.

TABLE 3

Results of electrochemical measurements in materials

Materials	Solutions	E_{corr} [V]	i_{corr} [mA cm^{-2}]
X20Cr13	0.1mol dm^{-3} H$_2$SO$_4$	-0.52	1.64
	0.5mol dm^{-3} H$_2$SO$_4$	-0.51	5.66
	0.5mol dm^{-3} Na$_2$SO$_4$	-0.51	0.028
	0.5mol dm^{-3} Na$_2$SO$_4$ + + 0.5mol dm^{-3} NaCl	-0.58	0.008
434LHC	0.1mol dm^{-3} H$_2$SO$_4$	-0.52	0.68
	0.5mol dm^{-3} H$_2$SO$_4$	-0.51	1.58
	0.5mol dm^{-3} Na$_2$SO$_4$	-0.55	0.001
	0.5mol dm^{-3} Na$_2$SO$_4$ + + 0.5mol dm^{-3} NaCl	-0.40	0.005

Comparison of the values of corrosion current density in the investigated environments reveals considerable reduction in corrosion rate in materials manufactured using powder metallurgy. The values of corrosion rate, depending on the investigated material and corrosion solution, are presented in Fig. 7.
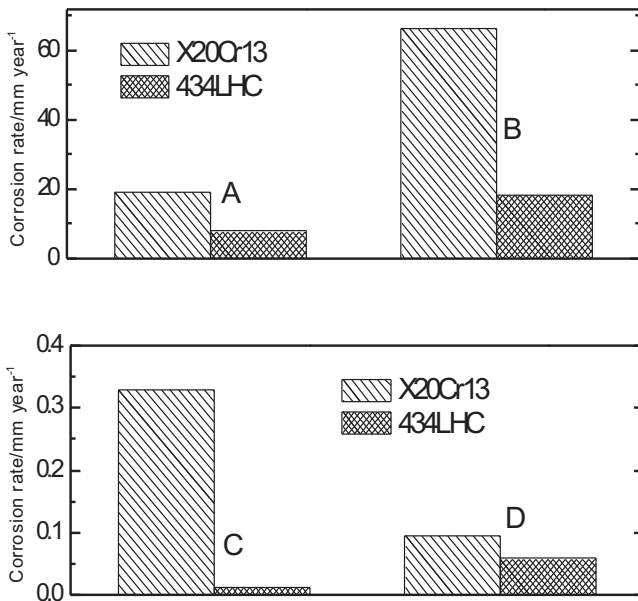
Fig. 7. Effect of the type of material on corrosion rate in the investigated solutions: 0.1mol dm^{-3} H$_2$SO$_4$ (A); 0.5mol dm^{-3} H$_2$SO$_4$ (B); 0.5mol dm^{-3} Na$_2$SO$_4$ (C); 0.5mol dm^{-3} Na$_2$SO$_4$ + 0.5mol dm^{-3} NaCl (D)

4. Summary

On the basis of the investigations, the following conclusions can be made:
- Stainless steel obtained by means of powder metallurgy (compaction and sintering) was characterized by 11% share of pores in the whole volume of material with regular pore shape and pore surface area within the range of 50 μm^2 to 100μm^2.
- Technology of material manufacturing (conventional method of steel manufacturing or powder metallurgy) affects values of corrosion current densities, however, does not considerably impact on corrosion potential in the investigated materials in sulphate solutions.
- In the solutions that contained chloride ions (responsible for pitting corrosion), sintered steel shows improved corrosion resistance as compared to X20Cr13 steel.
- The obtained structural investigations and high corrosion parameters allow for application of the proposed 434LHC sintered steel for fuel cell parts.

REFERENCES

[1] A. H e r m a n n, T. C h a u d h u r i, P. S p a g n o l, Int. J. Hydrogen Energy **30**, 1297 (2005).
[2] C. B e r n a y, M. M a r c h a n d, M. C a s s i r, J. Power Sources **108**, 139 (2002).
[3] E.R. D e l s m a n, C.U. U j u, M.H.J.M d e C r o o n, J.C. S c h o u t e n, K.J. P t a s i n s k i, Energy **31**, 3300 (2006).
[4] K. J a y a k u m a r, S. P a n d i y a n, N. R a j a l a k-s h m i, K.S. D h a t h a t h r e y a n, J. Power Sources **161**, 454 (2006).
[5] J. L a r m i n i e, A. D i c k s, Fuel Cell Systems Explained, Wiley & Sons, Ltd. 2003.
[6] N. S a m m e s, Fuel Cell Technology, Reaching Towards Commercialization, Springer, London, 2006.
[7] M.A.J. C r o p p e r, S. G e i g e r, D.M. J o l i e, J. Power Sources **131**, 57 (2004).
[8] R.L. B o r u p, N.E. V a n d e r b o r g h, Mater. Res. Soc. Symp. Proc. **393**, 151 (1995).
[9] V. M e h t a, J.S. C o o p e r, J. Power Sources **114**, 32 (2003).
[10] J.S. C o o p e r, J. Power Sources **129**, 152 (2004).